Reversible Reduction of Oxygen to Peroxide Facilitated by Molecular Recognition

Nazario Lopez *et al.*

Science **335**, 450 (2012);
DOI: 10.1126/science.1212678

6. K. Gallo, G. Assanto, K. R. Parameswaran, M. M. Fejer, *Appl. Phys. Lett.* **79**, 314 (2001).
7. M. Soljačić, C. Luo, J. D. Joannopoulos, S. Fan, *Opt. Lett.* **28**, 637 (2003).
8. A. Rostami, *Opt. Laser Technol.* **39**, 1059 (2007).
9. S. K. Ibrahim, S. Bhandare, D. Sandel, H. Zhang, R. Noe, *Electron. Lett.* **40**, 1293 (2004).
10. J. Hwang *et al.*, *Nat. Mater.* **4**, 383 (2005).
11. S. Manipatruni, J. T. Robinson, M. Lipson, *Phys. Rev. Lett.* **102**, 213903 (2009).
12. Z. Yu, S. Fan, *Nat. Photonics* **3**, 91 (2009).
13. M. S. Kang, A. Butsch, P. S. J. Russell, *Nat. Photonics* **5**, 549 (2011).
14. B. E. Little, S. T. Chu, H. A. Haus, J. Foresi, J.-P. Laine, *J. Lightwave Technol.* **15**, 998 (1997).
15. Q. Xu, B. Schmidt, S. Pradhan, M. Lipson, *Nature* **435**, 325 (2005).
16. S. Xiao, M. H. Khan, H. Shen, M. Qi, *Opt. Express* **15**, 14467 (2007).
17. S. Xiao, H. Shen, M. H. Khan, M. Qi, *Conf. Lasers and Electro-Optics* CTuGG6 (2008); www.opticsinfobase.org/abstract.cfm?uri=CLEO-2008-CTuGG6.
18. T. Barwicz *et al.*, *Opt. Express* **12**, 1437 (2004).
19. M. H. Khan *et al.*, *Nat. Photonics* **4**, 117 (2010).
20. M. Soljačić, M. Ibanescu, S. G. Johnson, Y. Fink, J. D. Joannopoulos, *Phys. Rev. E* **66**, 055601 (2002).
21. P. E. Barclay, K. Srinivasan, O. Painter, *Opt. Express* **13**, 801 (2005).
22. T. Uesugi, B.-S. Song, T. Asano, S. Noda, *Opt. Express* **14**, 377 (2006).
23. Q. Xu, M. Lipson, *Opt. Lett.* **31**, 341 (2006).
24. J. Ouyang, X. Wang, M. Qi, Meep (MIT Electromagnetic Equation Propagation), http://nanohub.org/resources/2954 (2007).
25. See supporting material on *Science* Online.
26. V. R. Almeida, M. Lipson, *Opt. Lett.* **29**, 2387 (2004).
27. P. Sun, R. M. Reano, *Opt. Lett.* **35**, 1124 (2010).
28. X. Chen, N. C. Panoiu, I. Hsieh, J. I. Dadap, R. M. Osgood, *IEEE Photon. Technol. Lett.* **18**, 2617 (2006).
29. J. B. Driscoll *et al.*, *IEEE J. Sel. Top. Quantum Electron.* **16**, 1448 (2010).
30. M. Dinu, F. Quochi, H. Garcia, *Appl. Phys. Lett.* **82**, 2954 (2003).
31. A. C. Turner-Foster *et al.*, *Opt. Express* **18**, 3582 (2010).

Acknowledgments: We thank D. Leaird for experimental assistance and J. Ouyang for helpful discussions. Supported by Defense Threat Reduction Agency grant HDTRA1-10-1-0106, Air Force Office of Scientific Research grant FA9550-08-1-0379, NSF grant ECCS-0925759, and NIH grant 1R01RR026273-01. Finite-difference time domain simulation work was carried out through the Network for Computational Nanotechnology with resources available at www.nanohub.org. L.F. and L.T.V. fabricated and characterized the devices. J.W. performed simulation and selected device parameters. H.S. helped in device characterization. B.N. helped in the design. M.Q. conceived the idea and supervised the investigation. M.Q., L.T.V., L.F., and J.W. wrote the manuscript. All discussed the results and commented on the manuscript.

Supporting Online Material

www.sciencemag.org/cgi/content/full/science.1214383/DC1
Materials and Methods
Table S1

23 September 2011; accepted 6 December 2011
Published online 22 December 2011;
10.1126/science.1214383

Reversible Reduction of Oxygen to Peroxide Facilitated by Molecular Recognition

Nazario Lopez,[1] Daniel J. Graham,[1] Robert McGuire Jr.,[1] Glen E. Alliger,[1] Yang Shao-Horn,[2] Christopher C. Cummins,[1]* Daniel G. Nocera[1]*

Generation of soluble sources of peroxide dianion (O_2^{2-}) is a challenge in dioxygen chemistry. The oxidizing nature of this anion renders its stabilization in organic media difficult. This Report describes the chemically reversible reduction of oxygen (O_2) to cryptand-encapsulated O_2^{2-}. The dianion is stabilized by strong hydrogen bonds to N-H groups from the hexacarboxamide cryptand. Analogous stabilization of peroxide by hydrogen bonding has been invoked recently in crystalline saccharide and protein systems. The present peroxide adducts are stable at room temperature in dimethyl sulfoxide (DMSO) and *N*,*N*′-dimethylformamide (DMF). These adducts can be obtained in gram quantities from the cryptand-driven disproportionation reaction of potassium superoxide (KO_2) at room temperature.

Reduction of molecular oxygen to the level of peroxide dianion (O_2^{2-}) is typically accomplished in chemical and biological systems in the stabilizing coordination sphere of a transition metal (*1*). Such peroxide transition-metal complexes are important intermediates in natural oxidation processes (*2*–*4*), and they have long been used as reagents for organic synthesis (*5*). We hypothesized that peroxide dianion could be stabilized alternatively in a molecular environment of hydrogen bond donors so arranged as to completely surround O_2^{2-} with partial positive charge. A structural basis for peroxide stabilization via hydrogen bonding to organic matter has appeared recently in the context of sodium peroxide crystallization with 1,6-anhydro-β-maltose (*6*). The reported complex salt of formula $[Na_2(1,6\text{-anhydro-}\beta\text{-maltose})_2(H_2O)_3]O_2$ has a layered structure featuring six hydrogen bonds that encase each O_2^{2-} ion, with sugar O-H groups acting as the hydrogen-bond donors. This peroxide environment is reminiscent of that determined for $Na_2O_2 \cdot 8\,H_2O$, in which chains of edge-connected $[Na(OH_2)_6]^+$ octahedra are linked together by O–H···O peroxide/water hydrogen bonds (*7*). Now, we show that hexacarboxamide cryptand molecules of a type introduced originally as receptors for halide ions (*8*, *9*), and investigated by us as binucleating ligands for transition-metal ions (*10*, *11*), form soluble 1:1 complexes with peroxide dianion wherein O_2^{2-} resides in a molecular interior surrounded by six carboxamide N-H hydrogen bond donors in a trigonal antiprismatic array. The receptors stabilize peroxide dianion to such an extent that, if it is present in the same solution, superoxide (O_2^-) undergoes disproportionation to form O_2 and encapsulated O_2^{2-}, thus coupling the anion receptor molecular recognition phenomenon (*12*) to an oxidation-reduction process.

Preparation of the cryptand peroxide adduct can be achieved starting from either superoxide or O_2. Treatment of a slurry of *tert*-butyl–substituted hexacarboxamide cryptand (*m*BDCA-5t-H_6) with 2.2 equiv of KO_2 in *N*,*N*′-dimethylformamide (DMF) resulted in the formation of the O_2^{2-} adduct $[K_2(DMF)_5][(O_2)\subset m\text{BDCA-5t-}H_6]$ in 74% isolated yield (Fig. 1). Vigorous bubbling was observed immediately after adding KO_2; mass spectrometry (MS, fig. S1) establishes that the gas is a result of O_2 production from the cryptand-driven disproportionation of O_2^-. The ^{1}H nuclear magnetic resonance (NMR) spectrum (fig. S2) indicates the formation of a O_2^{2-} adduct in which the amide chemical shift is in the range of a normal charged hydrogen bond (NCHB) interaction (*13*). The generality of peroxide dianion recognition was probed by using the related 3,5-dipropoxyphenoxyl–substituted hexacarboxamide cryptand (*m*BDCA-5p-H_6) (*10*). Similar large downfield shifts of ^{1}H NMR signals for N-H [14.69 parts per million (ppm)] and aromatic protons (10.03 ppm) pointing inside the cavity were observed, indicative of O_2^{2-} encapsulation at room temperature (fig. S3). The $[(O_2)\subset m\text{BDCA-5t-}H_6]^{2-}$ adduct can also be obtained by reducing O_2 in situ with 2 equiv of cobaltocene ($CoCp_2$, where Cp is cyclopentadienyl) in the presence of 1 equiv of free cryptand in DMF (fig. S4), where the first reduction potential of $CoCp_2$ is coincident with the reduction of oxygen (fig. S5).

Both cryptand peroxide adducts were characterized by x-ray diffraction studies using single crystals obtained by vapor diffusion of diethyl ether into DMF solutions (Fig. 2 and figs. S6 and S7). A view down the pseudo-threefold axis of the adduct indicates that the cryptand adopts a propeller-like conformation (Fig. 2B and fig. S7b). The O–O bond lengths of 1.504 ± 0.0002 [1.504(2) (number in parentheses indicates the estimated standard deviation in the final digit) Å for $[K_2(DMF)_5][(O_2)\subset m\text{BDCA-5t-}H_6]$ and 1.499(2) Å for $(DMF)[K_2(DMF)_5][(O_2)\subset m\text{BDCA-5p-}H_6]$, which are comparable to that in ribonucleotide reductase Ib (1.47 Å) (*14*), in 1,6-anhydro-β-maltose adduct [1.496(2) Å] (*6*), and in Na_2O_2 (1.49 Å)

[1]Department of Chemistry, 77 Massachusetts Avenue, Massachusetts Institute of Technology (MIT), Cambridge, MA 02139–4307, USA. [2]Departments of Mechanical Engineering and Materials Science and Engineering, 77 Massachusetts Avenue, MIT, Cambridge, MA 02139–4307, USA.

*To whom correspondence should be addressed. E-mail: nocera@mit.edu (D.G.N.); ccummins@mit.edu (C.C.C.)

(*15*), are indicative of the peroxide character of the O_2 moiety. Both structures reveal identical interactions with O_2^{2-} where the complementarity of the six amide protons with the six lone pairs on the peroxide dianion results in N···O distances in the range of 2.64 to 2.73 Å and 2.63 to 2.71 Å for $[K_2(DMF)_5][(O_2)\subset m\text{BDCA-5t-H}_6]$ (table S1) and $(DMF)[K_2(DMF)_5][(O_2)\subset m\text{BDCA-5p-H}_6]$ (table S3), respectively, which are indicative of strong hydrogen bonds (*16*). The amide protons of the present cryptand adducts are directed toward the lone pairs on the peroxide with N···O–O angles ranging from 117.7° to 123.8° and from 118.3° to 121.9° for $[K_2(DMF)_5][(O_2)\subset m\text{BDCA-5t-H}_6]$ (table S1) and $(DMF)[K_2(DMF)_5][(O_2)\subset m\text{BDCA-5p-H}_6]$ (table S3), respectively (*17*). The aryl protons pointing inside the cavity also interact with peroxide, with C···O distances ranging from 3.16 to 3.23 Å and from 3.13 to 3.18 Å for $[K_2(DMF)_5][(O_2)\subset m\text{BDCA-5t-H}_6]$ (table S2) and $(DMF)[K_2(DMF)_5][(O_2)\subset m\text{BDCA-5p-H}_6]$ (table S4), respectively, distances indicative of weak hydrogen bonds (*16*). Thus, the peroxide dianion is stabilized by a combination of six strong hydrogen bonds to six amide protons and six weak hydrogen bonds to three aryl protons (Fig. 2 and Table 1).

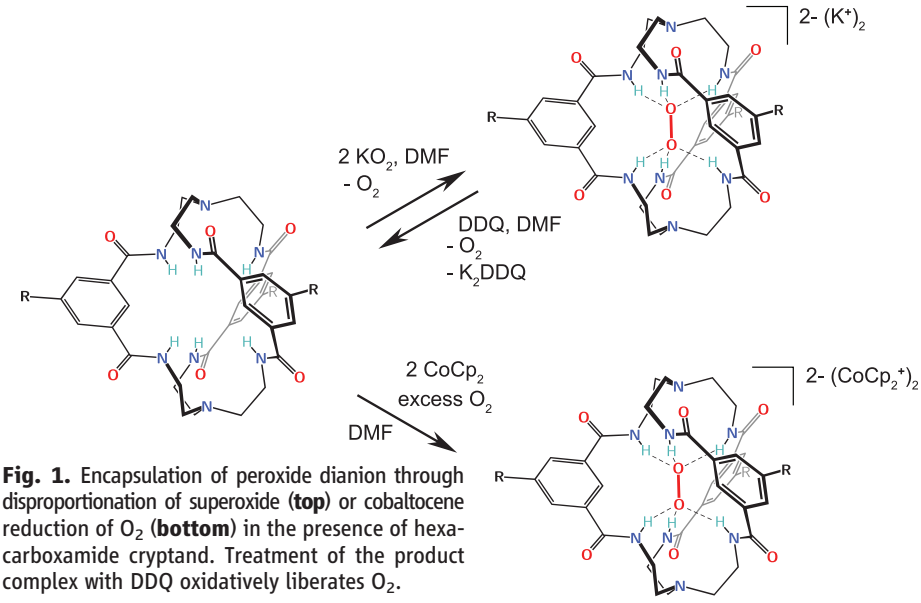

Fig. 1. Encapsulation of peroxide dianion through disproportionation of superoxide (**top**) or cobaltocene reduction of O_2 (**bottom**) in the presence of hexacarboxamide cryptand. Treatment of the product complex with DDQ oxidatively liberates O_2.

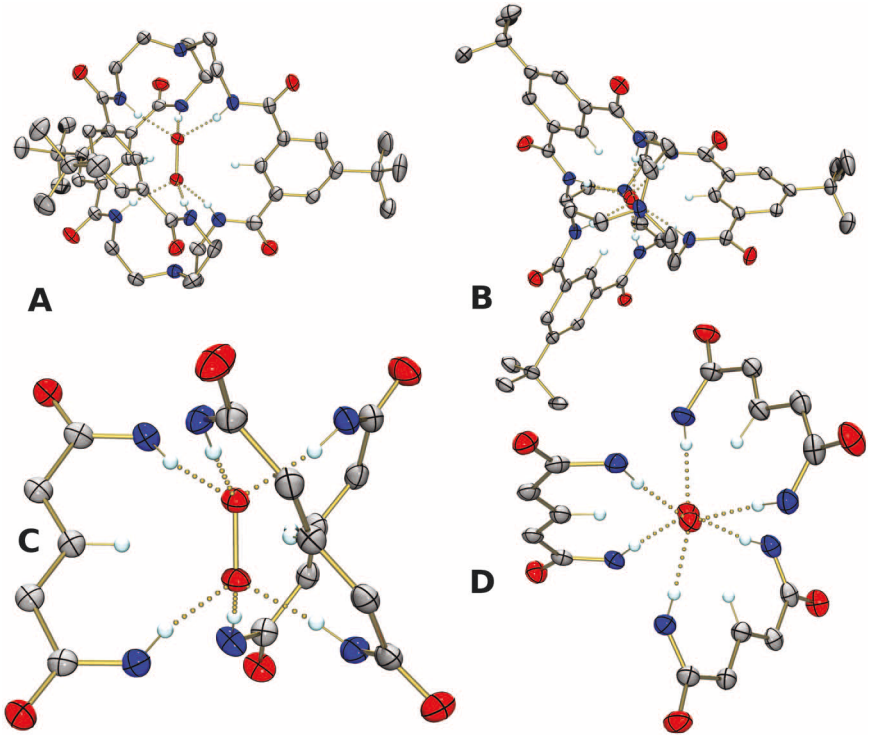

Fig. 2. Thermal ellipsoid plots at 50% probability level of $[K_2(DMF)_5][(O_2)\subset m\text{BDCA-5t-H}_6]$ peroxide adduct. (**A**) Side view and (**B**) view down the pseudo-threefold axis. Potassium ions, non–hydrogen-bonded hydrogen atoms, and DMF molecules have been omitted for clarity. (**C**) Side view and (**D**) view down the pseudo-threefold axis of cropped cryptand emphasizing the hydrogen-bonding interactions (dotted lines) with peroxide dianion. C is in gray; N, blue; O, red; H, light blue. Bond distance for $O\text{–}O_{peroxide}$ is 1.504(2) Å.

$[K_2(DMF)_5][(O_2)\subset m\text{BDCA-5t-H}_6]$ is stable in solution at room temperature for at least 1 month and remains intact even after heating for 100 min at 50°C (fig. S8). The molecular recognition of O_2^{2-} is reversible. Treatment of a solution containing 1 equiv of $[K_2(DMF)_5][(O_2)\subset m\text{BDCA-5t-H}_6]$ with 2 equiv of ferrocenium trifluoromethanesulfonate (FcOTf) results in quantitative production of free cryptand and ferrocene as indicated by ^{1}H NMR spectroscopy; no oxidation of the cryptand was observed (figs. S9 and S10). The cryptand fluoride adduct (*9*) is readily obtained through treatment of 1 equiv of $[K_2(DMF)_5][(O_2)\subset m\text{BDCA-5t-H}_6]$ with the convenient two-electron oxidant and fluoride source, xenon difluoride (XeF_2) (*18*) (figs. S11 and S12). The fluoride adduct, [TBA][(F)⊂*m*BDCA-5t-H_6] (TBA is tetra-*n*-butylammonium cation), was independently obtained and structurally characterized (figs. S13 to S15). The fluoride is hydrogen-bonded to all amide protons and three aryl protons as is observed for the peroxide adduct. The behavior of $[K_2(DMF)_5][(O_2)\subset m\text{BDCA-5t-H}_6]$ upon chemical oxidation was found to depend on the nature of the oxidant. No gaseous products were observed upon addition of 2 equiv of FcOTf to $[K_2(DMF)_5][(O_2)\subset m\text{BDCA-5t-H}_6]$. Although gas chromatography (GC) and MS revealed substantial CO_2 and Xe but insignificant O_2 in the headspace above dimethyl sulfoxide (DMSO) solutions of $[K_2(DMF)_5][(O_2)\subset m\text{BDCA-5t-H}_6]$ after treatment with XeF_2, the slow addition of 1.1 equiv 2,3-dichloro-5,6-dicyano-1,4-benzoquinone (DDQ) resulted in the sole release of O_2 in 88% yield as determined by GC (fig. S16) and MS (fig. S17). Analysis of the reaction mixture by ^{1}H NMR spectroscopy indicates that DDQ^{2-} is hydrogen-bonded to *m*BDCA-5t-H_6 (fig. S18); this interaction can be overcome by the formation of the fluoride adduct $[(F)\subset m\text{BDCA-5t-H}_6]^-$ when 2 equiv of [TBA][F] are added (fig. S19).

Evidence for the release of O_2 upon oxidation of $[K_2(DMF)_5][(O_2)\subset m\text{BDCA-5t-H}_6]$ at a glassy carbon electrode was obtained from a 4.8 mM solution of cryptand peroxide adduct in DMF containing 0.1 M $[TBA][ClO_4]$ by using a rotating ring disk electrode, scanning the potential of the disk, and holding the ring potential constant (fig. S20). During a potential scan of the disk electrode, a collection current is observed only when the ring is fixed to a potential sufficient for O_2 reduction. In addition, the release of O_2 is observed in cyclic voltammograms of the same solution. Although no features are observed

during an initial scan to negative potentials, a reductive wave appears only after oxidation of the complex at the electrode (fig. S21).

The observed chemical reactivity for reversible peroxide encapsulation is supported by the electrochemistry of the cryptand in the presence of oxygen. The reduction of oxygen to O_2^- solvated by large cations such as TBA is reversible in aprotic solvents (*19*). Whereas *m*BDCA-5t-H_6 shows no redox features from 0.25 to –2.3 V versus Ag/Ag^+, several new features are observed in the cyclic voltammograms of the cryptand in the presence of oxygen as shown in Fig. 3A. Upon scanning cathodically, an additional sharp reduction wave appears positive of the free-oxygen reduction wave at ~–1.4 V. The red trace shows the reversible one-electron oxygen/superoxide (O_2/[TBA][O_2]) couple in the absence of *m*BDCA-5t-H_6. On the return anodic sweep, a broad oxidation process is observed, centered at –0.7 V, in addition to the oxidation of free superoxide ([TBA][O_2]) at ~–1.4 V. The current associated with these new reduction and oxidation waves increases with increasing concentration of the cryptand, whereas the oxidation associated with superoxide ([TBA][O_2]) decreases.

Table 1. Selected hydrogen-bonding distances (Å) and angles (°).

Donor – – – H···Acceptor	D – H	H···A	D···A	D–H···A (°)
N101 – – H101 ··O2	0.86(2)	1.85(2)	2.692(3)	168(3)
N102 – – H102 ··O1	0.88(2)	1.83(2)	2.698(3)	169(3)
N201 – – H201 ··O2	0.87(3)	1.78(3)	2.639(3)	168(3)
N202 – – H202 ··O1	0.89(2)	1.84(2)	2.708(3)	168(2)
N301 – – H301 ··O2	0.88(3)	1.87(3)	2.732(3)	168(3)
N302 – – H302 ··O1	0.87(2)	1.80(2)	2.659(3)	167(3)

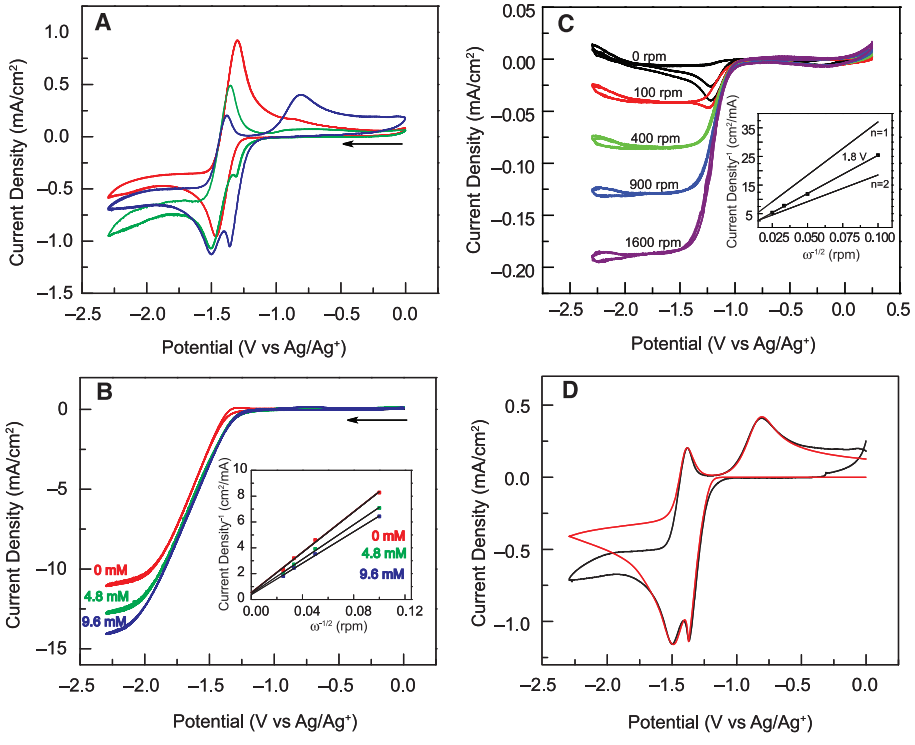

Fig. 3. (**A**) Cyclic voltammograms measured at a glassy carbon electrode in O_2-saturated DMF containing 0.1 M [TBA][ClO_4] in the presence of 0.0 mM *m*BDCA-5t-H_6 (red), 4.8 mM *m*BDCA-5t-H_6 (green), and 9.6 mM *m*BDCA-5t-H_6 (blue) (scan rate of 10 mV/s). (**B**) Rotating-disk electrode measurements using a glassy carbon electrode in O_2-saturated DMF containing 0.1 M [TBA][ClO_4] in the presence of 0.0 mM *m*BDCA-5t-H_6 (red), 4.8 mM *m*BDCA-5t-H_6 (green), and 9.6 mM *m*BDCA-5t-H_6 (blue) at 1600 revolutions per minute (rpm) (scan rate 100 mV/s). (Inset) K-L analysis of rotating-disk electrode data at 2.25 V for 0.0 mM *m*BDCA-5t-H_6 (red), 4.8 mM *m*BDCA-5t-H_6 (green), and 9.6 mM *m*BDCA-5t-H_6 (blue). (**C**) Rotating-disk electrode measurements using a glassy carbon electrode in DMF containing 0.1 M [TBA][ClO_4] saturated with 1% O_2 in argon in the presence of 4.8 mM *m*BDCA-5t-H_6 at 0 rpm (black), 100 rpm (red), 400 rpm (green), 900 rpm (blue), or 1600 rpm (purple) (scan rate 100 mV/s). (Inset) K-L analysis of rotating-disk electrode data at 1.8 V and the expected slopes for $n = 1$ and $n = 2$. (**D**) Cyclic voltammogram of 9.6 mM *m*BDCA-5t-H_6 (black) and simulated cyclic voltammogram (red) using the mechanistic steps described in Fig. 4.

On the basis of the reaction chemistry depicted in Fig. 1, we propose that the new reduction wave results from the ability of the cryptand to rapidly sequester O_2^- formed at the cathode and facilitate subsequent transfer of a second electron from either the electrode or another molecule of O_2^-. The sharp decrease in current responsible for the shape of the peak is indicative of the rapid depletion of free cryptand near the electrode, a phenomenon that is due to the ease with which the cryptand reacts with O_2^- and the sluggish diffusion of free cryptand to the electrode relative to free O_2. As the working electrode potential decreases further, one-electron reduction of O_2 produces a steady supply of O_2^-, which can react with free cryptand as it diffuses away from the electrode. Measurements of independently prepared [K_2(DMF)$_5$][(O_2)⊂*m*BDCA-5t-H_6] in argon-saturated solution show predominant oxidation at ~–0.7 V and subsequent reduction at ~–1.4 V, which support observations indicating that these two features correspond to the oxidation of the cryptand peroxide with concomitant release of O_2 and the reformation of [(O_2)⊂*m*BDCA-5t-H_6]$^{2-}$, respectively (fig. S21). Measurements of oxygen reduction in the presence of tris(2-aminoethyl) amine (TREN) or 5-*tert*-butylisophthalic acid (figs. S22 and S23) show negligible oxidation currents from ~–1.5 to ~–0.5 V, indicating that the oxidation process at ~–0.7 V is not cryptand-based and that the cryptand remains intact during the oxygen redox measurements. Overall, the process is electrochemically irreversible under saturated oxygen.

Rotating-disk electrode measurements further confirm that the cryptand drives the O_2 reduction to a two-electron process. Figure 3B and figs. S24 to S26 show the rotating-disk electrode results for increasing concentration of *m*BDCA-5t-

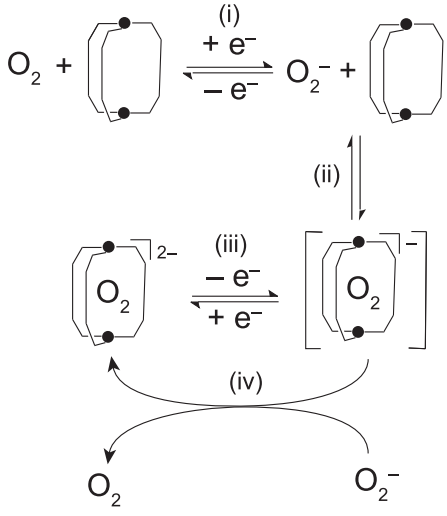

Fig. 4. Proposed mechanism of the reversible cryptand-facilitated O_2 reduction to encapsulated O_2^{2-}. Simulated standard potentials, rate constants, and equilibrium constants for the elementary steps labeled i to iv were derived from fits to the cyclic voltammetry data and are given in table S5a.

H_6 and *m*BDCA-5p-H_6 in oxygen-saturated DMF solution. An increase in the limiting current as well as decreasing slope of the Koutecký-Levich (K-L) analysis of diffusion-limited currents (Fig. 3B, inset) is consistent with a greater number of electrons transferred during reduction of oxygen in the presence of *m*BDCA-5t-H_6 than the one-electron reduction process without *m*BDCA-5t-H_6 (*20*). A large excess of cryptand is needed in order to drive the electrochemical process completely to peroxide encapsulation during rotating-disk electrode experiments. K-L analysis of diffusion-limiting currents as a function of the inverse square root of rotation speed, collected in 0.1 M [TBA][ClO_4] DMF solution saturated with 1% O_2 in argon with 4.8 mM *m*BDCA-5t-H_6 (Fig. 3C), indicates that the number of transferred electrons increases toward an overall two-electron process, which is expected if every oxygen molecule was reduced and encapsulated by the cryptand.

Figure 3D shows a simulation of the cyclic voltammogram using the reaction sequence illustrated in Fig. 4. The reaction sequence used to model the electrochemistry concurs with the established chemical reactivity of O_2 and cryptand described by Fig. 1. Parameters obtained from the simulation are collected in table S5, a and b. Our model suggests that rapid encapsulation of O_2^- by free cryptand drives further one-electron reduction, either directly by the working electrode or through a disproportionation reaction with another equiv of O_2^-, resulting in the formation of $[(O_2)\subset m\text{BDCA-5t-H}_6]^{2-}$. The assumption that the diffusion coefficient of O_2 is much greater than that of the cryptand species (table S5b) in DMF containing 0.1 M [TBA][ClO_4] reproduces the sharp feature observed before the wave attributed to one-electron reduction of O_2. An appropriate fit for the anodic sweep could only be accomplished by modeling the oxidation of $[(O_2)\subset m\text{BDCA-5t-H}_6]^{2-}$ as a series of two, one-electron oxidations.

The reversible one-electron reduction of oxygen in DMF is altered by addition of both strong and weak acids (*21*). In the case of *m*BDCA-5t-H_6, the cryptand could serve as a source of protons. However, figs. S27 and S28 illustrate that the reduction of oxygen in the presence of strong and weak acids, respectively, differs from oxygen reduction in the presence of *m*BDCA-5t-H_6 at equal concentration. These data suggest that the cryptand does not serve as a Brønsted acid in the overall oxygen reduction process.

The electrochemistry of *m*BDCA-5t-H_6 and *m*BDCA-5p-H_6 in the presence of oxygen is consistent with reduction of oxygen by one electron to superoxide followed by incorporation into the cryptand cavity, in turn driving disproportionation to give the cryptand-encapsulated peroxide adduct. Oxidation of peroxide dianion within the cavity restores oxygen and the free cryptand ligand. The proposed electrochemical mechanism in Fig. 4 maps on to the observed chemical reactivity of Fig. 1; the combined chemical and electrochemical studies demonstrate encapsulation-driven chemically reversible two-electron reduction of O_2 to peroxide dianion.

We have synthesized a molecular peroxide dianion adduct by the use of the cavity of hexacarboxamide cryptands as a molecular recognition site. Reduction of oxygen in situ and stabilization of peroxide dianion is facilitated by hydrogen bonding within the cavity of the cryptand, and this process mimics the structural characteristics of biological systems that use peroxide as an oxidant. The use of molecular recognition of an in situ–generated reactive oxygen species has the potential to be incorporated into several technologies, including Li-air batteries, because it is chemically reversible, prevents overreduction to lithium oxide, and imparts substantial solubility in aprotic media (*22*). In addition, because the present peroxide adducts can be obtained in high yield in a one-pot reaction and are stable in solution, they could be used as a soluble source of peroxide dianion for a variety of reactions.

References and Notes

1. B. Meunier, Ed., *Metal-Oxo and Metal-Peroxo Species in Catalytic Oxidations* (Springer, Berlin, 2000).
2. B. Meunier, Ed., *Biomimetic Oxidations Catalyzed by Transition Metal Complexes* (Imperial College Press, London, 2000).
3. B. Meunier, S. P. de Visser, S. Shaik, *Chem. Rev.* **104**, 3947 (2004).
4. A. Butler, M. J. Clague, G. E. Meister, *Chem. Rev.* **94**, 625 (1994).
5. M. V. George, K. S. Balachandran, *Chem. Rev.* **75**, 491 (1975).
6. T. Kato *et al.*, *Chem. Lett.* **39**, 136 (2010).
7. M. Grehl, R. Fröhlich, S. Thiele, *Acta Crystallogr. C* **51**, 1038 (1995).
8. S. O. Kang, J. M. Llinares, D. Powell, D. VanderVelde, K. Bowman-James, *J. Am. Chem. Soc.* **125**, 10152 (2003).
9. S. O. Kang, V. W. Day, K. Bowman-James, *J. Org. Chem.* **75**, 277 (2010).
10. G. E. Alliger, P. Müller, C. C. Cummins, D. G. Nocera, *Inorg. Chem.* **49**, 3697 (2010).
11. G. E. Alliger, P. Müller, L. H. Do, C. C. Cummins, D. G. Nocera, *Inorg. Chem.* **50**, 4107 (2011).
12. J. L. Sessler, P. A. Gale, W.-S. Cho, *Anion Receptor Chemistry* (Royal Society of Chemistry, London, ed. 1, 2006).
13. M. Garcia-Viloca, A. González-Lafont, J. M. Lluch, *J. Am. Chem. Soc.* **119**, 1081 (1997).
14. A. K. Boal, J. A. Cotruvo Jr., J. Stubbe, A. C. Rosenzweig, *Science* **329**, 1526 (2010).
15. R. D. Jones, D. A. Summerville, F. Basolo, *Chem. Rev.* **79**, 139 (1979).
16. G. R. Desiraju, T. Steiner, in *The Weak Hydrogen Bond in Structural Chemistry and Biology* (Oxford Univ. Press, Oxford, 1999), p. 13.
17. The residual electron density of refinements without assignment of the electron density of N-H hydrogen atoms surrounding the peroxide moiety suggests that the protons reside at the carboxamide nitrogens of the cryptand, even though the exact position cannot be obtained from x-ray data. Thus, hydroperoxide anion HO_2^- is unlikely to be the species trapped, and the best model obtained was of peroxide dianion (figs. S29 to S32).
18. N. Bartlett, F. O. Sladky, *Chem. Commun.* **1968**, 1046 (1968).
19. D. L. Maricle, W. G. Hodgson, *Anal. Chem.* **37**, 1562 (1965).
20. A. J. Bard, L. R. Faulkner, in *Electrochemical Methods: Fundamentals and Applications* (Wiley, New York, ed. 2, 2000), p. 341.
21. D. T. Sawyer, G. Chiericato Jr., C. T. Angelis, E. J. Nanni Jr., T. Tsuchiya, *Anal. Chem.* **54**, 1720 (1982).
22. G. Girishkumar, B. McCloskey, A. C. Luntz, S. Swanson, W. Wilcke, *J. Phys. Chem. Lett.* **1**, 2193 (2010).

Acknowledgments: This research was supported by the NSF–Centers for Chemical Innovation (CHE-0802907). Grants from the NSF also provided instrument support to the Department of Chemistry Instrument Facility at MIT (grants CHE-9808061 and DBI-9729592). D.J.G. thanks the NSF Graduate Research Fellowship Program for support. We thank Y. Surendranath for productive discussions and collecting mass spectrometry data, A. F. Cozzolino and P. Müller for structure refinement discussions, and F. A. Armstrong for helpful discussions. Complete crystallographic data were deposited in the Cambridge Crystallographic Database Centre (CCDC 831953 to 831955 and 831962).

Supporting Online Material

www.sciencemag.org/cgi/content/full/335/6067/450/DC1
Materials and Methods
Figs. S1 to S32
Tables S1 to S5
References (*23*–*27*)

15 August 2011; accepted 13 December 2011
10.1126/science.1212678

A Long-Lived Lunar Core Dynamo

Erin K. Shea,[1]* Benjamin P. Weiss,[1] William S. Cassata,[2] David L. Shuster,[2,3] Sonia M. Tikoo,[1] Jérôme Gattacceca,[4] Timothy L. Grove,[1] Michael D. Fuller[5]

Paleomagnetic measurements indicate that a core dynamo probably existed on the Moon 4.2 billion years ago. However, the subsequent history of the lunar core dynamo is unknown. Here we report paleomagnetic, petrologic, and $^{40}Ar/^{39}Ar$ thermochronometry measurements on the 3.7-billion-year-old mare basalt sample 10020. This sample contains a high-coercivity magnetization acquired in a stable field of at least ~12 microteslas. These data extend the known lifetime of the lunar dynamo by 500 million years. Such a long-lived lunar dynamo probably required a power source other than thermochemical convection from secular cooling of the lunar interior. The inferred strong intensity of the lunar paleofield presents a challenge to current dynamo theory.

The discovery of remanent magnetization in samples taken by the Apollo lunar missions and by spacecraft observations of the lunar crust has long suggested that the Moon formed a metallic core and a dynamo-generated magnetic field (*1*). However, the association of magnetization with the antipodes of impact basins and laboratory studies of transient plasma-generated magnetic fields suggest that meteoroid impacts could also be a source of lunar magnetization (*2, 3*).